Available online at www.sciencedirect.com
ScienceDirect
Acta Materialia 55 (2007) 5348–5358
Acta MATERIALIA
www.elsevier.com/locate/actamat

Initiation of shear bands near a stress concentration in metallic glass

C.E. Packard, C.A. Schuh *

Department of Materials Science and Engineering, Massachusetts Institute of Technology, Cambridge, MA 02139, USA

Received 16 May 2007; received in revised form 29 May 2007; accepted 29 May 2007
Available online 2 August 2007

Abstract

Instrumented contact experiments are performed on three metallic glasses to systematically study shear band formation near a stress concentration. The results suggest that high local stresses at a point in the glass are insufficient to initiate a shear band. Rather, the yield strength must be exceeded along the entire length of a viable shear path in order for a shear band to form. Because of this, conventional analyses to extract shear yield stresses from Hertzian contact experiments overestimate the glass strength by a factor of three or more. In contrast, the interpretation of shear band initiation as yield on a plane agrees with recent experimental observations on metallic glasses that pertain to the slip-line field, and can rationalize the experimental contact load measurements as well as the shear band path.
© 2007 Acta Materialia Inc. Published by Elsevier Ltd. All rights reserved.

Keywords: Metallic glasses; Shear bands; Stress concentration; Nanoindentation

1. Introduction

Metallic glasses have several properties attractive in structural materials, such as high yield strength, high hardness, and reasonable fracture toughness [1]. However, before metallic glasses are seriously considered for use in load bearing applications, their yield and fracture behavior must be better understood. This is especially true in light of their strong tendency for flow localization at low temperatures, which leads to abrupt quasi-brittle mechanical failure along shear bands [2,3]. The discrete accommodation of deformation in shear bands complicates our understanding of the deformation process, and the conditions to initiate, sustain, and arrest flow on a shear band remain unclear. Consequently, there is a growing interest in the plasticity of metallic glasses evident in the literature [4–12].

Many studies have aimed to increase the ductility or toughness of metallic glasses [4,5,7,12]. For example, Lewandowski et al. [8] and others [6,11] have shown how subtle changes in chemical composition or structure can affect the elastic properties of a glass, which in turn appear to correlate with toughness. Other studies have explored the macroscopic stresses achieved when shear bands first form under uniaxial conditions; these exhibit a tension/compression asymmetry [12,13] that is also reflected in more complex multiaxial stress states [11,14–16]. Other groups have studied plasticity around crack tips [17–22] or surface contacts [23–26], giving important insights into shear band formation under complex stress states. Finally, the introduction of metallic glass composites containing second phases [4,5,7,18,27] raises fundamental questions as to how such reinforcements can interfere with shear bands and affect fracture toughness and ductility [4,7,27,28]. This wide range of approaches shows that researchers are clearly interested in understanding and controlling the mechanism of plastic deformation in metallic glasses.

Though some significant progress has been made in recent years using the techniques described above, the process of shear band formation in metallic glasses remains somewhat mysterious [29]. Several fundamental aspects of shear banding are still under intense debate. For example, the temperature rise associated with shear banding has received considerable attention, with some studies proposing an increase of just a few degrees and others concluding

* Corresponding author.
E-mail address: schuh@mit.edu (C.A. Schuh).

1359-6454/$30.00 © 2007 Acta Materialia Inc. Published by Elsevier Ltd. All rights reserved.
doi:10.1016/j.actamat.2007.05.054

that temperatures sufficiently high to cause melting are achieved [30–35]. An underlying uncertainty that contributes to this confusion is that the actual geometry/thickness of a shear band remains unknown, owing to the difficulty of resolving features in amorphous materials with conventional microscopy techniques [36–38]. Claims of shear band thicknesses ranging from 10 nm to nearly micron-scale exist in the literature [37–40]. Also under debate are the issues of shear band arrest and the possibility of "work hardening" in metallic glasses at obstacles such as particles, voids, or shear bands from prior deformation [4,41,42]. Even the basic sequence of events by which a bona fide shear band evolves from an initial collection of local shear transformation zones remains essentially speculative [2,43–49].

Among the above uncertainties about shear band formation, there is a pressing need to understand how shear bands form in complex stress fields, especially near stress concentrations [50]. This information is not only instrumental to the design of structures made from metallic glass, but to provide underpinning physics for problems of fracture and fatigue, and motivate the rational design of glass composite microstructures. The purpose of the present work is to systematically study shear band formation near a stress concentration. As this study is aimed at understanding the fundamental aspects of the first stages of deformation, we restrict our attention to a simple and well-understood geometry; specifically, we explore shear band initiation at a Hertzian surface contact. Experimental results from several glasses are analyzed and a criterion is proposed to describe the conditions required to initiate a shear band in metallic glass. This criterion not only rationalizes the experimental contact load measurements, but also the shear band path beneath a Hertzian contact.

2. Experiments

Three bulk metallic glasses were used in this study: one of each based on Pd, Zr, and Fe; the exact compositions of the alloys are listed in Table 1. Each specimen was several millimeters in diameter, produced by arc melting pure metals and casting into cooled copper molds under an inert atmosphere, as detailed in [51–53]. Specimens were metallographically sectioned and mechanically polished to a roughness of less than 5 nm for contact mechanical studies in a nanoindenter.

In order to introduce a well-defined stress concentration and to have the capability of detecting shear band formation, we performed instrumented Hertzian contact experiments. The Hertzian spherical contact geometry provides a well-known elastic stress field prior to yield, while the instrumented indentation test platform allows ready detection of shear banding events, which are accompanied by displacement bursts [54–57]. All of the experiments were performed using a Nanomechanical Test Instrument (from Hysitron, Inc., Minneapolis, MN, USA) with load and depth resolution of 0.1 μN and 0.2 nm, respectively. Three diamond tips were used for this study, and over the range of indentation depths considered here, each tip was approximately spherical. The radius of curvature was determined for each of the tips using standard techniques [58–60], giving tip radii of $R = 180$, 590, and 1100 nm. For each set of experiments with a particular tip and sample combination, the indenter was loaded to a specified maximum load at a constant rate of 0.15 mN s^{-1}.

Fig. 1 illustrates the basic responses measured in our experiments, with Fig. 1a showing data from a typical indentation in the Pd-based glass with the $R = 590$ nm tip. Loading and unloading at low loads in the elastic range labeled in Fig. 1a produced no measurable plastic deformation, with the unloading curve exactly retracing the loading curve. However, once the load exceeded some critical threshold, rapid depth excursions were observed in the loading curves as denoted by the large filled points in Fig. 1a. These "pop-ins" correspond to shear banding events, as commonly seen in nanoindentation experiments [55–57,61]. The occurrence of the first pop-in marks the onset of plastic flow; indentations beyond this point always exhibited measurable residual displacements after unloading.

The separation of shear banding events from elastic deflection is also made clear by comparing the data to a Hertzian elastic prediction [62,63] of the load–displacement relationship,

$$P = \frac{4}{3} E_r R^{1/2} h^{3/2}, \tag{1}$$

where P is the load, R is the radius of the indenter tip, h is the indentation depth, and E_r is the reduced modulus. The reduced modulus is given by

$$\frac{1}{E_r} = \frac{1 - \nu_{sample}^2}{E_{sample}} + \frac{1 - \nu_{indenter}^2}{E_{indenter}}, \tag{2}$$

Table 1
Compositions and relevant properties for the glasses used in this study

Composition	E_r (GPa)	Poisson's ratio	Vickers hardness (GPa)	τ_y from Vickers (GPa)	$\sigma_{y,c}$ (GPa)	τ_y from $\sigma_{y,c}$ (GPa)
$Pd_{40}Ni_{40}P_{20}$	117 ± 1	0.4 [90]	5.1 ± 0.1	0.7	1.4 – 1.78 [10,13]	0.6 – 0.8
$Fe_{41}Co_7Cr_{15}Mo_{14}C_{15}B_6Y_2$	217 ± 2	0.3[a] [6,91]	11.7 ± 0.4	1.6	3.5 [65]	1.5
$Zr_{49}Cu_{45}Al_6$	109 ± 2	0.36[a] [91]	5.1 ± 0.1	0.7	1.2 – 1.5 [66]	0.5 – 0.7

Error bars on τ_y are liberally assigned as ±20%.
[a] Approximate value from glasses of similar composition.

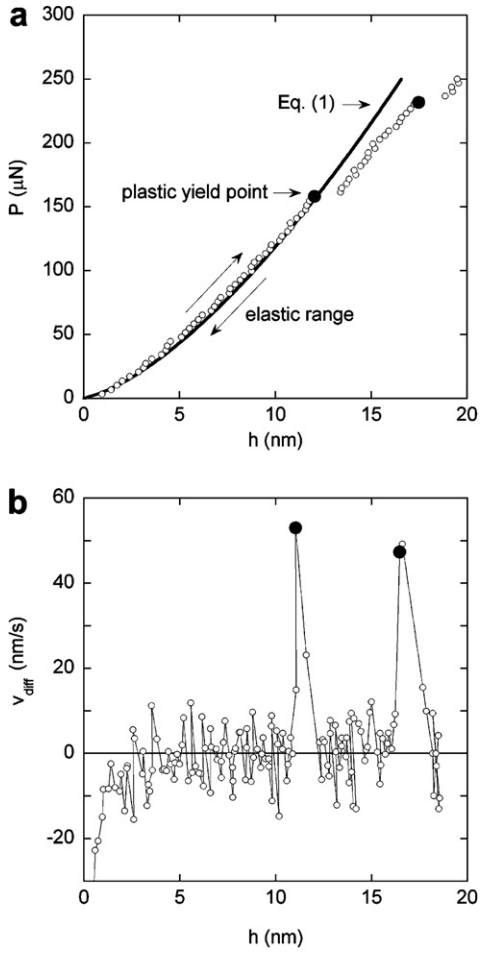

Fig. 1. Instrumented Hertzian contact response during loading of the Pd-based glass using a 590 nm tip radius. (a) Typical load–depth response demonstrating departure from the elastic prediction of Eq. (1) at the plastic yield point. Sudden depth excursions in (a), represented by darkened circles, correspond exactly to spikes in the velocity response shown in (b) during shear banding events.

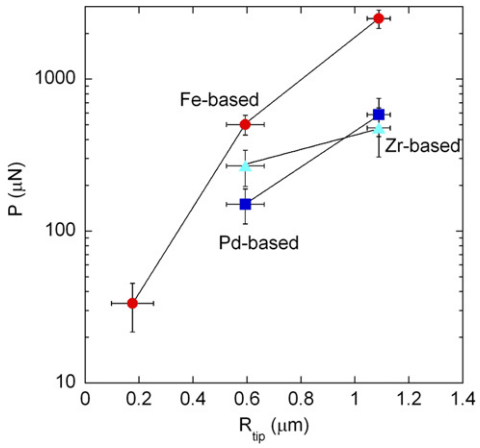

Fig. 2. Average load for the first shear banding event in three metallic glasses for several test geometries. Each data point represents an average of over 100 individual first yield points, identified using the techniques illustrated in Fig. 1.

where E is the Young's modulus and ν is Poisson's ratio for the sample and diamond indenter tip, as denoted by the subscripts. Fig. 1a illustrates the expected elastic response for the Pd-based glass, using the elastic constants from Table 1 along with the values for diamond from Ref. [64]. The agreement between Eq. (1) and the experimental data is further evidence that the deflection prior to the first pop-in is indeed elastic. The indenter velocity (dh/dt) predicted for a strictly Hertzian elastic contact can also be subtracted from the true indentation velocity to reveal pop-ins as a sudden spike in the differential velocity, v_{diff}. Fig. 1b shows a typical measurement of v_{diff} corresponding to the load–displacement curve from Fig. 1a, where such spikes are shown to be significantly higher in magnitude than the noise [54]. In Fig. 1b, the filled data points correspond exactly to those from Fig. 1a.

In this study we focus on the stress state required to initiate the first shear band in these experiments. For each combination of glass and indenter tip, many nominally identical indentations were performed to obtain statistically reliable information about the first shear banding event. The first event was identified for each test using both of the criteria outlined above: (1) a sudden depth excursion marking the first departure from the Hertzian prediction, and (2) a corresponding spike in the velocity. Fig. 2 compiles our results, showing the measured load P at the yield point. Each data point is an average of more than 100 individual tests conducted under identical test conditions. Vertical error bars mark the standard deviations of the measurements, while horizontal error bars denote the uncertainty in the tip radius. A semi-logarithmic format is chosen solely to help illustrate trends.

3. Analysis

We divide our purpose in the following discussion into two subgoals:

(1) We aim to understand the stress state at yield, and quantitatively relate the measurements in Fig. 2 to the known macroscopic yield stresses of the three glasses. Amorphous metals are elastically isotropic and the measurements in Fig. 2 represent the first departure from elastic behavior, so we can reasonably assume that the stress state in the material at the moment immediately prior to yield is precisely known and described by the Hertzian contact equations. Using the Hertzian model, we shall seek a connection between the stress state at yield, and independent macroscopic measurements of the shear yield stress, τ_y. Values of τ_y for the glasses studied here are compiled in Table 1, based on compressive yield stress measurements from the literature [10,13,65,66] as well as Vickers hardness measurements using 200 g load for 15 s. Uniaxial and hardness data were converted to shear yield stresses according to Refs. [67,68], incorporating a normal stress dependence described

by the Mohr–Coulomb yield criterion. The estimated shear yield stresses listed in Table 1 are assigned liberal error bars that account for uncertainty in the measurements, as well as the range of material-specific constants used in the stress conversions. Although these values are thus somewhat approximate, we shall see shortly that they are sufficiently accurate for our purposes.

(2) We intend to specifically link the stress state at yield with the geometry of a forming shear band. Here we wish to identify how the shear band path is affected by a stress concentration. Since we cannot directly observe events that occur in the interior of the specimen during deformation, we look to post-deformation photographic evidence, which is fortunately available from a variety of prior works on indentation of metallic glasses [68–72]. For example, Fig. 3 is an image of the deformation field around a cylindrical indentation in a Zr-based glass from Ref. [71]. While this photograph is for a cylindrical geometry and our experiments use a spherical one, the mechanical similarities are sufficient to make some important qualitative observations. For example, as shown by the dotted line in Fig. 3, for a given contact radius a, shear bands penetrate deeply into the material to a depth in excess of 2a. In what follows, we will use the dashed line from Fig. 3 as an approximate shear band path to compare with the predictions of various models.

With the above two goals in mind, the following sections discuss several proposals for analyzing the yield condition around a Hertzian stress concentration. We begin with a common procedure used to analyze indentation data, motivated by work on crystalline metals, and show that for metallic glasses a new framework is required. We then review an existing model for yield of amorphous metals around a Hertzian contact, and finally propose a condition that properly captures the nature of yield as a shear band formation event. This condition rationalizes both our measurements in Fig. 2 and observations of shear band paths such as those from Fig. 3.

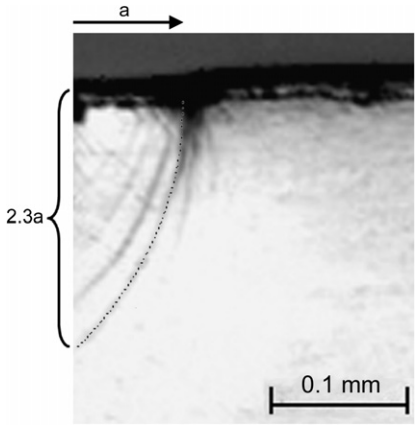

Fig. 3. Shear bands around a cylindrical indentation from Ref. [71] penetrate to a depth of more than twice the contact radius. The dashed line here is reproduced in later figures as an example.

3.1. Maximum shear stress criterion

The simplest starting point for analyzing yield around a Hertzian contact is to consider the maximum shear stress sustained in the material immediately prior to yield. This approach is common for crystalline metals [54,58,73–77], and is predicated on the ideas that (i) yielding is controlled by shear stresses, and (ii) the location where the stresses are highest will correspond to the dominant initiation point. This approach is used for its relative simplicity and its success in explaining the onset of plasticity in several material systems in which there is a discrete nucleation-type event that triggers plastic flow [54,58,73–77]. For a variety of crystalline materials, the predictions of this approach have been related to theoretical yield stresses or stresses associated with specific physical events such as dislocation nucleation [54,58,74,76,77]. It is of specific interest to note that Bei et al. [59] applied this approach to interpret nanoindentation results on a metallic glass.

For elastic contact of a sphere on a flat plate, a complete solution for the stress state throughout the indented material is available, based on the original model of Hertz [78]. Identifying the characteristic length scale of the problem with the contact radius,

$$a = \left(\frac{3PR}{4E_r}\right)^{1/3} \tag{3}$$

and the characteristic stress with the mean contact pressure,

$$P_m = \frac{4}{3}\frac{E_r a}{\pi R}, \tag{4}$$

the full solution for the Hertzian stress field can be expressed in reduced stresses (σ') and spatial variables (r', z') in cylindrical coordinates around the first contact point, where the prime denotes normalization by Eq. (3) or (4). For convenience, we reproduce the full set of equations for the various stress components beneath the contact in Appendix A. Using these equations, the maximum (σ'_1) and minimum (σ'_3) principal stresses can be used to compute the maximum shear stress (τ') at every point in the stress field according to

$$\tau'(r',z') = \frac{1}{2}\left(\sigma'_1 - \sigma'_3\right). \tag{5}$$

The right side of Fig. 4 shows contours of the maximum shear stress (Eq. (5)) throughout the elastic half-space. From this plot, it is seen that a point along $r' = 0$ at a depth of $z' \sim 0.5$ experiences the highest shear stress in the material. The maximum shear stress present at this point may be expressed in approximate form as

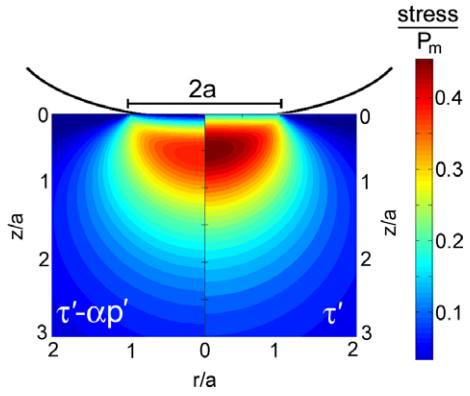

Fig. 4. Stress field under a Hertzian contact. Contours of maximum shear stress (τ') and pressure-modified shear stress ($\tau' - \alpha p'$ with $\alpha = 0.12$) are shown on the right and left, respectively. The pressure modification reduces the maximum stress and shifts it slightly deeper into the material.

$$\tau_{max} \approx 0.45 \cdot P_m, \tag{6}$$

where the numerical prefactor assumes a Poisson's ratio of $\nu = 0.33$. Using Eq. (6) with Eq. (4), a load measurement from a contact experiment can be converted into the maximum shear stress, and more precise conversions for known values of ν are possible using the full field equation (Eq. (5)) with Eq. (4).

We have extracted the value of τ_{max} at yield from each individual contact experiment underlying the data in Fig. 2, using the values for Poisson's ratio found in Table 1. The resulting maximum shear stresses obtained using this method are shown in Fig. 5a. The conversion from loads to stresses (P vs. τ_{max} in Figs. 2 and 5a, respectively) adequately scales out the trends with tip radius; the yield stress in Fig. 5a is relatively constant with R for each experimental material. However, in each case the extracted yield stresses are extremely high, significantly exceeding the macroscopic shear yield stresses for these glasses, which are listed in Table 1 and shown as horizontal bars in Fig. 5. The error bars on our results (from more than 100 tests at each set of conditions) are very small compared to the disagreement reflected here.

Thus, one problem with assigning τ_{max} as the yield stress in this situation is that it returns values that are quite drastically out of line with respect to the expected values. A second serious problem with this approach is revealed by considering the expected shear band trajectory, were yield to initiate from the position of maximum shear stress at $z' \sim 0.5$. Comparing Figs. 3 and 4, it is clear that shear bands beneath Hertzian contacts penetrate much more deeply than $z' = 0.5$, to depths beyond $z' = 2$. More detailed quantitative analysis of the expected shear band path highlights this discrepancy. The path of a shear band originating from the point of maximum shear stress has been calculated based on the full Hertzian stress field according to the procedure outlined in Appendix B. This trajectory is shown as a black line in Fig. 6, where we also reproduce the dotted line indicating the shear band path from Fig. 3. Clearly, the observed shear band traverses significantly more volume than that predicted by the maximum shear stress method.

Though the maximum shear stress yield criterion has been applied to other situations with considerable success (particularly for crystalline materials), for metallic glasses we are unable to even approximately match the expected yield stress, or rationalize the trajectories of the shear bands with this criterion. These data therefore suggest that shear bands do not simply initiate when a large shear stress is present at a point in a stress concentration field.

3.2. Pressure-modified criterion

Plastic deformation has been found to exhibit a significant pressure or normal stress dependence in metallic glasses, as evidenced by tension/compression asymmetry in the yield stress [9,13,79], and deviations in the shear and fracture planes from the planes of maximum shear stress [10,12,69,79–81]. It seems possible, therefore, that the confining pressure beneath a Hertzian contact could

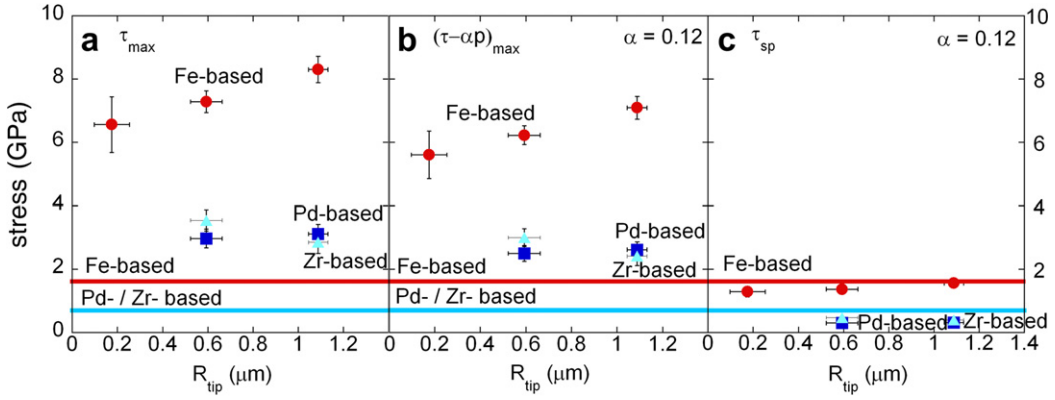

Fig. 5. Results of converting the critical indentation loads into stress values, with shaded bars indicating the macroscopic shear yield stresses from Table 1. In (a) the maximum shear stress criterion from Section 3.1 is used to calculate the stress, and in (b) the pressure-modified shear stress from Section 3.2 is presented; these criteria lead to very high values of extracted yield stress. In (c), the shear plane stress based on the analysis in Section 3.3 is shown, giving extracted yield stresses that are more in line with the expected values (horizontal bars).

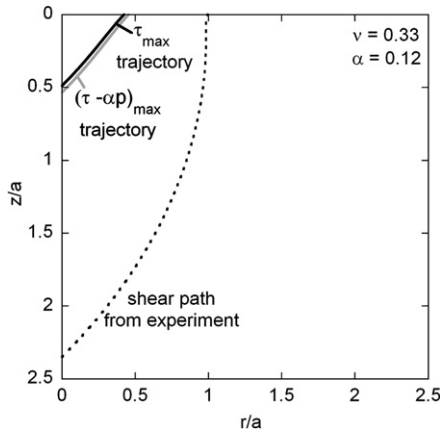

Fig. 6. The predicted shear trajectory for a yield event controlled by the maximum shear stress (solid black line), or by the maximum pressure-modified shear stress (solid gray line). For comparison a typical observed shear band path beneath a Hertzian contact is also shown.

suppress shear band formation and force the initiation point deeper into the material. Therefore, a next logical step to analyzing our contact measurements is to incorporate the effect of a pressure or normal stress into the yield criterion. A first attempt to incorporate such effects into the τ_{max} analysis described in the previous section was reported by Wright et al. [82]. In their analysis, the Hertz model was still employed, but the normal stress on an assumed shear plane was incorporated into the yield criterion, and a procedure was presented to identify the yield stress by solving a system of equations. The procedure we outline below alternatively uses a pressure-dependent yield strength. However, we have performed the same analysis using the normal stress modification proposed by Wright et al., and find no significant difference in the final result.

The pressure can be computed at any point in the Hertzian field from the principal stress components,

$$p'(r',z') = -\frac{\sigma'_r + \sigma'_z + \sigma'_\theta}{3}. \tag{7}$$

We then define a pressure-modified maximum shear stress as

$$\tau' - \alpha \cdot p', \tag{8}$$

and plot this field on the left side of Fig. 4, using a pressure coefficient of $\alpha = 0.12$. Comparison to the maximum shear stress field (on the right of Fig. 4) shows that pressure slightly shifts the field, which attains a maximum at a marginally larger depth ($z' \sim 0.54$ as compared with $z' \sim 0.5$), and lowers the effective stress levels everywhere. An approximation for the maximum pressure-modified stress present in the material can be expressed in the same form as Eq. (6),

$$(\tau - \alpha p)_{max} \approx 0.41 \cdot P_m, \tag{9}$$

for the specific case where $\nu = 0.33$ and $\alpha = 0.12$.

Fig. 5b shows the maximum pressure-modified stresses extracted from each of our measurements, using the appropriate values for Poisson's ratio from Table 1 and an assumed pressure coefficient $\alpha = 0.12$. The stresses obtained according to this criterion are somewhat reduced compared with the maximum shear stress estimates from Fig. 5a, but are still significantly higher than the true shear yield stress; the error is still more than a factor of two, and the extracted yield stresses remain physically implausible. Fig. 6 shows the trajectory originating from the point of maximum pressure-modified stress as a gray line. Since the stress field shifts only slightly due to the pressure dependence, the trajectory of the shear band only shifts a correspondingly small amount. In other words, a pressure-modified yield criterion is insufficient to explain the very deep shear bands observed in experiments, as shown by the dotted line in Fig. 6, if we continue to assume that yield initiates at the point of maximum stress.

Thus, the introduction of a pressure-modified yield stress does little to resolve the problems seen in the previous section; neither the extracted stress levels nor the shear band trajectory match the expected response. Although the addition of a pressure effect shifts the results in the correct direction, its effect is subtle. This result is not an artifact of the specific assumptions used here. For example, as mentioned above, the use of a normal stress instead of a pressure dependence gives essentially the same results; the theoretical shear trajectory shifts only slightly, and the extracted stresses are still much too high. What is more, the specific choice of $\alpha = 0.12$ can be regarded as an effective upper bound on the pressure effect, this being one of the highest reported values for α [29]; the predictions in Fig. 6 cannot be improved with any physically reasonable choice of α. Thus, we conclude that even when confining stresses are accounted for, considering only the highest stresses at a point in the material fails to accurately describe the conditions for shear band formation around a stress concentrator.

3.3. Shear plane criterion

In our view, the reason that the above analyses fail is that they do not acknowledge the process of shear band formation as a cooperative effect that occurs on a specific shear plane. For example, it has been pointed out for several years [57,69,83–87] that the shear band fields observed in experiments on metallic glasses closely match those expected from classical slip-line field analysis of rigid perfectly plastic materials. In such materials, the yield event is shearing on a plane over which a yield stress is everywhere exceeded. We propose that analysis of the elastic–plastic transition in metallic glasses must conform to these observations. In what follows, we examine the stresses along various potential shear paths, and posit that the plane sustaining the highest stress *along its entire path* is the preferred shear plane, the minimum stress along that path defining the yield strength.

We begin by analyzing the stress along various possible shear band trajectories. Using the approach outlined in

Appendix B, several example shear trajectories originating along the z-axis have been plotted in Fig. 7a. The shape of a trajectory depends on its starting coordinates, and the stress is not constant along it; instead it traverses the stress field shown in Fig. 4. Fig. 7b shows how the effective shear stress (pressure-modified) varies along the several paths illustrated in Fig. 7a, where the left-hand side of the plot represents $r' = 0$, and the trajectories terminate (the right of the plot) when they reach the surface. From Fig. 7b, it is apparent that paths i and ii reach very high stresses at local points along their length, but it can also be seen that other points along these paths experience minimal stresses. Although its stress profile is more complex, a similar statement may be made about path iv, which also experiences very low stresses over part of its length. In contrast, path iii, though it does not achieve extremely high stresses anywhere on its length, experiences a sustained moderate stress level of at least $0.07P_m$ along the entire trajectory. If the yield stress must be exceeded everywhere along the shear plane in order for a shear band to form, then path iii is the only viable candidate from among these four.

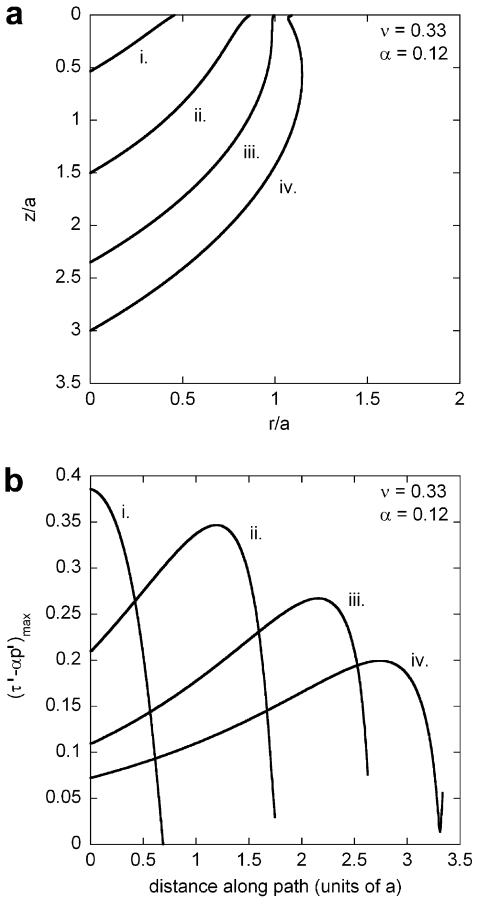

Fig. 7. (a) Potential shear band trajectories calculated according to Appendix B and (b) the stress along those trajectories as they traverse the stress field starting from $r' = 0$. Some paths reach very high stresses locally, but elsewhere on the path the stresses are very low. Path iii sustains the highest stress over its entire length.

To exhaustively consider all possible shear paths around the contact zone, we have computed trajectories from a multitude of starting coordinates over the range of $r' = [0, 5]$ and $z' = [0, 5]$ and the stress $(\tau - \alpha p)$ at each point along a given path was determined. We define the minimum pressure-modified stress along a given path as τ_{sp}, which we view to be the effective yield stress for shear on a plane. Normalized values of τ_{sp} are plotted as a function of the spatial origin of the shear trajectory in Fig. 8. The main feature of Fig. 8 is a narrow path of high τ_{sp} extending from $z' \sim 2.3$ to the edge of the contact near $r' \sim 1$; based on its high shear plane stress, this path emerges as the preferential trajectory. This trajectory does not experience the highest stresses in the Hertzian field, but is the only trajectory stressed above the critical stress for yield along its entire length. Comparing Figs. 8 and 3, it is encouraging to see that this criterion can adequately explain the very deep shear bands that are known to form around Hertzian contacts.

We propose that the trajectory in Fig. 8 is the one that is activated during the first pop-in event and that τ_{sp} along that path is the controlling stress for yield. Because this trajectory specifically does not traverse the highest stresses in the field (cf. Fig. 4), τ_{sp} is necessarily much lower than τ_{max}. To compare the various yield analyses studied here, we plot the major result from each in Fig. 9, along the z-axis. In this figure, the maximum shear stress τ and pressure-modified stress $(\tau - \alpha p)$ both demonstrate a maximum value near $z' \sim 0.5$ that is a significant fraction of the mean contact pressure – as high as 0.45 and 0.41, respectively (see also Eqs. (6) and (9)). Alternatively, τ_{sp} is considerably

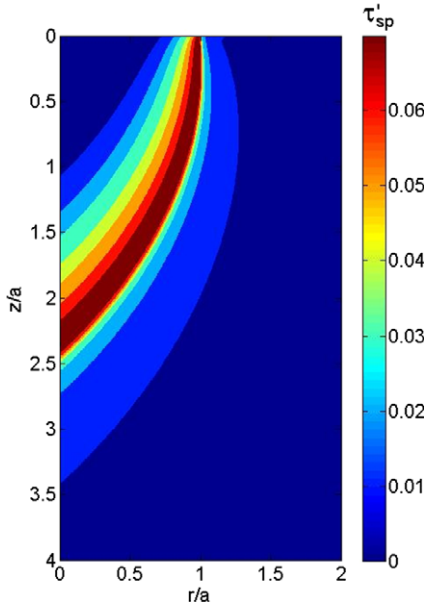

Fig. 8. Shear plane stresses plotted as a function of the spatial origin of each potential trajectory. The shear path from $z' \sim 2.3$ emerges as the preferential trajectory because it sustains the highest stress over the entire path length. This result compares well to the shear band path observed in Fig. 3.

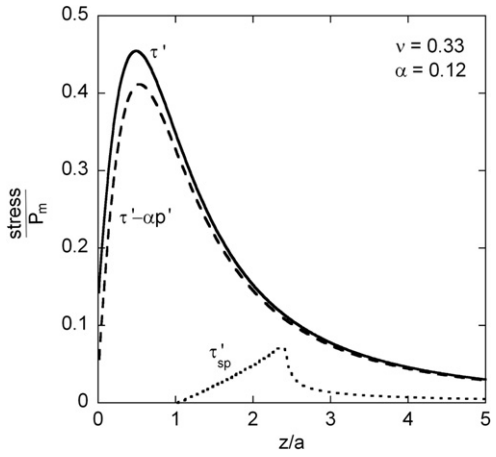

Fig. 9. The three proposed yield-controlling stresses are plotted along the $r' = 0$ axis for comparison. Although the local point stresses τ' and $\tau' - \alpha p'$ maximize near $z' = 0.5$, the shear plane stress τ_{sp} (defined as the minimum stress along the shear path emanating from a given point) predicts that shear band formation will occur much deeper in the material ($z' \sim 2.3$), and at a lower stress.

lower at all z', and predicts that shear banding will occur at a much more moderate stress level of

$$\tau_{sp} \approx 0.07 \cdot P_m \tag{10}$$

over the entire trajectory spanning from $z' \sim 2.3$ to the edge of the contact circle.

Fig. 5c plots the results of applying this shear plane criterion to the measurements from Fig. 2. Here we have maintained the vertical scale used in Fig. 5a and b for consistency in comparing the results obtained using the various analysis methods. In contrast to those of Fig. 5a and b using the maximum shear or pressure-modified shear stress criteria, the results in Fig. 5c are of the correct order, and in light of the liberal error bars we have assigned to the "true" values of shear yield stress (Table 1), the agreement with the data is quite good. In fact, it is encouraging to see that this analysis returns yield strengths somewhat lower than do macroscopic tests. In the present scenario, the yield point is not sequestered in the bulk beneath the impression site, but actually involves a shear band connecting to the free surface. For small-scale contact tests like these, surface imperfections would then be expected to lower the measured strength. Accordingly, the results in Fig. 5c are eminently plausible as compared with those in either Fig. 5a or b.

Based on the results in Fig. 5c and the location of the resulting predicted shear plane from Fig. 8, we conclude that shear band formation is governed by the development of high stresses along the entire length of a viable shear plane, and not by the highest stresses near a stress concentration, per se.

4. Implications and conclusions

In this paper, incipient strain localization was studied through instrumented Hertzian contact experiments in three metallic glass compositions. Measurements at yield were analyzed with existing methods based on local (point) stresses, without success. On the other hand, a shear plane condition in which the yield criterion must be satisfied everywhere on the shear plane rationalizes our contact measurements as well as observations of the shear band trajectory. The shear plane predicted by this analysis bears close resemblance to that expected from slip-line field theory [69,88,89], which has been successfully used to explain the geometry of shear bands around stress concentrations in metallic glasses [17,57,69,83–86].

Previous attempts to analyze Hertzian contact data in metallic glasses have used maximum local stress criteria, resulting in high values of the extracted yield stress [59,82]. For example, Bei et al. [59] reported yield stresses more than 3.5 times the actual shear yield strength for Zr-based glasses using the maximum shear stress criterion. Wright et al. [82] used a normal stress-modified criterion to analyze indentations on a different Zr-based glass, but still reported yield stresses up to three times the actual shear yield stress. Both of these studies suggested that the discrepancy was a consequence of testing stressed volumes so small that they were essentially "defect free". However, the reported yield stresses are so high in those works that it is difficult to rationalize such an increase through size effects. The shear yield stress of metallic glasses is already near the theoretical limit, and an additional factor of three seems physically unreasonable. What is more, those studies did not explicitly validate the proposed size effect by performing the same analysis at different indentation sizes, and in this work where we have done so, no such size effect was seen despite hundreds of tests in three different glasses (see Fig. 5). If anything, our data may be interpreted as showing a reverse size effect, in which smaller indentations return somewhat lower yield strengths. This observation aligns with our earlier comments about surface imperfections, which play an important role if the yield occurs not in the bulk beneath the indentation, but via a shear band that actually connects with the surface. As the indentation size is reduced, the relative importance of surface irregularities increases, and lower measured strengths could be expected. Finally, we observe that neither of the studies by Bei et al. or Wright et al. considered how a maximum point-stress criterion would incorrectly predict the shear band geometry.

Our analysis illustrates that local satisfaction of the yield criterion at a point is not sufficient to initiate shear banding, and this may have important implications. First, this result may speak to the underlying mechanism of shear band formation in metallic glasses as a fundamentally cooperative process. Whereas the operation of a shear transformation zone (STZ) requires the coordinated reshuffling of only dozens of atoms (nearly a "point" process within the material that should be responsive to the local stress field), the formation of a shear band would seem to require the involvement of many STZs operating in concert. As noted in Ref. [29], the nature of shear band

initiation has been the subject of some debate. Some researchers hold that a viable shear path forms first by the local assembly of many STZs, giving a band of material that has sustained a very small amount of displacement along its entire length; only subsequently are large displacements accumulated via relatively uniform shearing on the plane. Other authors favor a model in which a very large displacement is accumulated locally and then must propagate as a front. In the latter scenario the material is apparently more responsive to local stresses, which initiate a shear front at a specific location in space, and subsequently propagate it through the material. In that picture, it would seem that around a Hertzian contact, local (point) stresses would permit the initiation of the shear band at $z' \sim 0.5$, and it would then be required to propagate through a field of lower driving stresses. Such a model may be appropriate for, e.g., a perfect crystal, where a Hertzian indentation leads to dislocation nucleation after a large activation barrier is surmounted, and subsequent propagation of the already-formed defect requires substantially lower stresses. However, the present experimental results argue against such an interpretation for shear band formation in a metallic glass. That shear bands apparently avoid regions of high local stress in order to satisfy the yield criterion along an entire viable shear plane suggests a cooperative process of STZ assembly that may align with the first hypothesis above, i.e., that a shear path is first defined by cooperative assembly of STZs, followed by sustained uniform shearing on that path.

Second, these results may suggest new means of interpreting mechanical data for metallic glasses containing stress risers. For example, the classical notions of localized "microplasticity" preceding "macroscopic yield" [28] may be unusually distinct in metallic glasses, with microplasticity corresponding to fully confined STZ activity, and macroscopic yield corresponding to the selection of a shear path according to a shear-plane stress criterion. Use of conventional continuum mechanics analysis, without properly accounting for the deformation physics of shear banding, would fail to capture this distinction. Clearly, such considerations will be important for glasses with microstructural features, as well as in problems of fracture and fatigue.

Acknowledgements

This work was supported by the Office of Naval Research, Grant No. N00014-04-1-0669. The authors would like to thank Prof. Y. Li (National University of Singapore) and Prof. J. Shen (Harbin Institute of Technology) for providing the samples used in this investigation, as well as Prof. L. Anand (Massachusetts Institute of Technology) for providing the micrograph in Fig. 3.

Appendix A. Hertzian equations

The equations for the stress components involved in Hertzian spherical contact on a flat plate are found in Ref. [62]. Below, we present the equations for the nonzero stress components in a normalized form, where

$$\sigma' \equiv \sigma/P_{\mathrm{m}}, \quad r' \equiv r/a, \quad z' \equiv z/a, \tag{A1–A3}$$

$$\sigma'_{\mathrm{r}} = \frac{3}{2}\left\{\frac{1-2v}{3r'^2}\left[1-\left(\frac{z'}{\sqrt{u'}}\right)^3\right] + \left(\frac{z'}{\sqrt{u'}}\right)^3 \frac{u'}{u'^2+z'^2} + \frac{z'}{\sqrt{u'}}\left[u'\frac{(1-v)}{1+u'} + (1+v)\sqrt{u'}\tan^{-1}\left(\frac{1}{\sqrt{u'}}\right) - 2\right]\right\}, \tag{A4}$$

$$\sigma'_{\theta} = -\frac{3}{2}\left\{\frac{1-2v}{3r'^2}\left[1-\left(\frac{z'}{\sqrt{u'}}\right)^3\right] + \frac{z'}{\sqrt{u'}}\left[2v + u'\frac{(1-v)}{1+u'} - (1+v)\sqrt{u'}\tan^{-1}\left(\frac{1}{\sqrt{u'}}\right)\right]\right\}, \tag{A5}$$

$$\sigma'_{z} = -\frac{3}{2}\frac{z'^3}{\sqrt{u'}(u'^2+z'^2)}, \tag{A6}$$

$$\sigma'_{rz} = -\frac{3}{2}\frac{r'z'^2\sqrt{u'}}{(u'^2+z'^2)(1+u')}, \tag{A7}$$

where u' is the normalized displacement, defined as

$$u' = \frac{1}{2}\left[r'^2 + z'^2 - 1 + \left[\left(r'^2+z'^2-1\right)^2 + 4z'^2\right]^{1/2}\right]. \tag{A8}$$

The normalized principal stresses are calculated from

$$\sigma'_{1,3} = \frac{\sigma'_{\mathrm{r}}+\sigma'_z}{2} \pm \sqrt{\left(\frac{\sigma'_{\mathrm{r}}-\sigma'_z}{2}\right)^2 + \sigma'^2_{rz}}, \tag{A9}$$

$$\sigma'_2 = \sigma'_{\theta}. \tag{A10}$$

Appendix B. Evaluation of shear trajectories

We define a path function, f, which describes a trajectory through the material. The function can be expressed in differential form as

$$\mathrm{d}f(r',z') = \left(\frac{\partial f}{\partial r'}\right)\mathrm{d}r' + \left(\frac{\partial f}{\partial z'}\right)\mathrm{d}z'. \tag{B1}$$

To evaluate this equation, expressions for the partial derivatives are required. We assume that the angular direction of the path at every point is determined by the shear angle

$$\phi_{\mathrm{s}} = \tan^{-1}\left\{-\frac{\sigma'_{\mathrm{r}}-\sigma'_z}{2\sigma'_{rz}} \pm \left[\left(\frac{\sigma'_{\mathrm{r}}-\sigma'_z}{2\sigma'_{rz}}\right)^2 + 1\right]^{1/2}\right\} - \frac{\pi}{4}, \tag{B2}$$

where $\pm$ is the sign of σ_{rz}. This angle can be used to decompose incremental distances along the path Δf into their r' and z' components,

$$\Delta r' = \Delta f \cos\phi_{\mathrm{s}}, \tag{B3}$$

$$\Delta z' = \Delta f \sin\phi_{\mathrm{s}}. \tag{B4}$$

Upon rearrangement and taking the limit as the incremental path distance, Δf, becomes very small, the partial derivatives can be obtained as

$$\frac{\partial f}{\partial r'} = \sec\phi_s, \tag{B5}$$

$$\frac{\partial f}{\partial z'} = \csc\phi_s. \tag{B6}$$

With this information, Eq. (B1) may be numerically solved to obtain $f(r', z')$, the shear trajectory originating from any given starting point in the material.

References

[1] Ashby MF, Greer AL. Metallic glasses as structural materials. Scripta Mater 2006;54:321.

[2] Argon AS. Plastic-deformation in metallic glasses. Acta Metal 1979;27:47.

[3] Spaepen F. Microscopic mechanism for steady-state inhomogeneous flow in metallic glasses. Acta Metal 1977;25:407.

[4] Das J, Tang MB, Kim KB, Theissmann R, Baier F, Wang WH, et al. "Work-hardenable" ductile bulk metallic glass. Phys Rev Lett 2005:94.

[5] Fan C, Ott RT, Hufnagel TC. Metallic glass matrix composite with precipitated ductile reinforcement. Appl Phys Lett 2002;81:1020.

[6] Gu XJ, McDermott AG, Poon SJ, Shiflet GJ. Critical Poisson's ratio for plasticity in Fe–Mo–C–B–Ln bulk amorphous steel. Appl Phys Lett 2006:88.

[7] Hufnagel TC, Fan C, Ott RT, Li J, Brennan S. Controlling shear band behavior in metallic glasses through microstructural design. Intermetallics 2002;10:1163.

[8] Lewandowski JJ, Wang WH, Greer AL. Intrinsic plasticity or brittleness of metallic glasses. Philos Mag Lett 2005;85:77.

[9] Lund AC, Schuh CA. The Mohr–Coulomb criterion from unit shear processes in metallic glass. Intermetallics 2004;12:1159.

[10] Mukai T, Nieh TG, Kawamura Y, Inoue A, Higashi K. Effect of strain rate on compressive behavior of a $Pd_{40}Ni_{40}P_{20}$ bulk metallic glass. Intermetallics 2002;10:1071.

[11] Schroers J, Johnson WL. Ductile bulk metallic glass. Phys Rev Lett 2004:93.

[12] Sergueeva AV, Mara NA, Kuntz JD, Lavernia EJ, Mukherjee AK. Shear band formation and ductility in bulk metallic glass. Philos Mag 2005;85:2671.

[13] Donovan PE. A Yield Criterion for $Pd_{40}Ni_{40}P_{20}$ Metallic-Glass. Acta Metal 1989;37:445.

[14] Lewandowski JJ, Lowhaphandu P. Effects of hydrostatic pressure on the flow and fracture of a bulk amorphous metal. Philos Mag A 2002;82:3427.

[15] Ott RT, Sansoz F, Jiao T, Warner D, Fan C, Molinari JF, et al. Yield criteria and strain-rate behavior of $Zr_{57.4}Cu_{16.4}Ni_{8.2}Ta_8Al_{10}$ metallic-glass-matrix composites. Metall Mater Trans A 2006;37A:3251.

[16] Takayama S. Drawing of $Pd_{77.5}Cu_6Si_{16.5}$ metallic glass wires. Mater Sci Eng 1979;38:41.

[17] Flores KM, Dauskardt RH. Enhanced toughness due to stable crack tip damage zones in bulk metallic glass. Scripta Mater 1999;41:937.

[18] Lewandowski JJ, Shazly M, Nouri AS. Intrinsic and extrinsic toughening of metallic glasses. Scripta Mater 2006;54:337.

[19] Lowhaphandu P, Lewandowski JJ. Fracture toughness and notched toughness of bulk amorphous alloy: Zr–Ti–Ni–Cu–Be. Scripta Mater 1998;38:1811.

[20] Hajlaoui K, Yavari AR, Doisneau B, LeMoulec A, Botta WJF, Vaughan G, et al. Shear delocalization and crack blunting of a metallic glass containing nanoparticles: in situ deformation in TEM analysis. Scripta Mater 2006;54:1829.

[21] Zhou M, Rosakis AJ, Ravichandran G. On the growth of shear bands and failure-mode transition in prenotched plates: a comparison of singly and doubly notched specimens. Int J Plast 1998;14:435.

[22] Li JX, Shan GB, Gao KW, Qiao LJ, Chu WY. In situ SEM study of formation and growth of shear bands and microcracks in bulk metallic glasses. Mater Sci Eng A 2003;354:337.

[23] Hodge AM, Nieh TG. Evaluating abrasive wear of amorphous alloys using nanoscratch technique. Intermetallics 2004;12:741.

[24] Kishore, Sudarsan U, Chandran N, Chattopadhyay K. On the wear mechanism of iron and nickel based transition metal-metalloid metallic glasses. Acta Metall 1987;35:1463.

[25] Michler J, Rabe R, Bucaille JL, Moser B, Schwaller P, Breguet JM. Investigation of wear mechanisms through in situ observation during microscratching inside the scanning electron microscope. Wear 2005;259:18.

[26] Miyoshi KH, Buckley D. Mechanical-contact-induced transformation from the amorphous to the partially crystalline state in metallic glass. Thin Solid Films 1984;118:363.

[27] Hays CC, Kim CP, Johnson WL. Microstructure controlled shear band pattern formation and enhanced plasticity of bulk metallic glasses containing in situ formed ductile phase dendrite dispersions. Phys Rev Lett 2000;84:2901.

[28] Ott RT, Sansoz F, Molinari JF, Almer J, Ramesh KT, Hufnagel TC. Micromechanics of deformation of metallic-glass-matrix composites from in situ synchrotron strain measurements and finite element modeling. Acta Mater 2005;53:1883.

[29] Schuh CA, Hufnagel TC, Ramamurty U. Mechanical behavior of amorphous alloys. Acta Mater 2007;55:4067.

[30] Bailey NP, Schiotz J, Jacobsen KW. Atomistic simulation study of the shear-band deformation mechanism in Mg–Cu metallic glasses. Phys Rev B 2006;73:64108.

[31] Flores KM, Dauskardt RH. Local heating associated with crack tip plasticity in Zr–Ti–Ni–Cu–Be bulk amorphous metals. J Mater Res 1999;14:638.

[32] Lewandowski JJ, Greer AL. Temperature rise at shear bands in metallic glasses. Nature Mater 2006;5:15.

[33] Wright WJ, Schwarz RB, Nix WD. Localized heating during serrated plastic flow in bulk metallic glasses. Mater Sci Eng A 2001;319:229.

[34] Yang B, Morrison ML, Liaw PK, Buchanan RA, Wang G, Liu CT, et al. Dynamic evolution of nanoscale shear bands in a bulk-metallic glass. Appl Phys Lett 2005;86:141904.

[35] Zhang Y, Stelmashenko NA, Barber ZH, Wang WH, Lewandowski JJ, Greer AL. Local temperature rises during mechanical testing of metallic glasses. J Mater Res 2007;22:419.

[36] Jiang WH, Atzmon M. The effect of compression and tension on shear-band structure and nanocrystallization in amorphous $Al_{90}Fe_5Gd_5$: a high-resolution transmission electron microscopy study. Acta Mater 2003;51:4095.

[37] Li J, Spaepen F, Hufnagel TC. Nanometre-scale defects in shear bands in a metallic glass. Philos Mag A 2002;82:2623.

[38] Pekarskaya E, Kim CP, Johnson WL. In situ transmission electron microscopy studies of shear bands in a bulk metallic glass based composite. J Mater Res 2001;16:2513.

[39] Donovan PE, Stobbs WM. The structure of shear bands in metallic glasses. Acta Metall 1981;29:1419.

[40] Zhang Y, Greer AL. Thickness of shear bands in metallic glasses. Appl Phys Lett 2006:89.

[41] Bei H, Xie S, George EP. Softening caused by profuse shear banding in a bulk metallic glass. Phys Rev Lett 2006:96.

[42] Inoue A, Zhang W, Tsurui T, Yavari AR, Greer AL. Unusual room-temperature compressive plasticity in nanocrystal-toughened bulk copper-zirconium glass. Philos Mag Lett 2005;85:221.

[43] Argon AS. Mechanisms of inelastic deformation in metallic glasses. J Phys Chem Solids 1982;43:945.

[44] Cahn RW, Haasen P, Kramer EJ. Materials science and technology: a comprehensive treatment. Weinheim; New York: VCH; 1991.

[45] Ju L, Shimizu F, Ogata S. Yield point of metallic glass. Acta Mater 2006;54:4293.

[46] Langer JS. Shear-transformation-zone theory of deformation in metallic glasses. Scripta Mater 2006;54:375.
[47] Li Q-K, Li M. Atomic scale characterization of shear bands in an amorphous metal. Appl Phys Lett 2006;88:241903.
[48] Shi Y, Falk ML. Strain localization and percolation of stable structure in amorphous solids. Phys Rev Lett 2005;95:1.
[49] Steif PS, Spaepen F, Hutchinson JW. Strain localization in amorphous metals. Acta Metall 1982;30:447.
[50] Nieh TG, Liu CT, Wang WH, Pan M. Reflections on the third UEF conference on bulk metallic glasses. Intermetallics 2004;12:1033.
[51] Fu XL, Li Y, Schuh CA. Contributions to the homogeneous plastic flow of in situ metallic glass matrix composites. Appl Phys Lett 2005:87.
[52] Mukai T, Nieh TG, Kawamura Y, Inoue A, Higashi K. Dynamic response of a $Pd_{40}Ni_{40}P_{20}$ bulk metallic glass in tension. Scripta Mater 2002;46:43.
[53] Shen J, Chen QJ, Sun JF, Fan HB, Wang G. Exceptionally high glass-forming ability of an FeCoCrMoCBY alloy. Appl Phys Lett 2005:86.
[54] Mason JK, Lund AC, Schuh CA. Determining the activation energy and volume for the onset of plasticity during nanoindentation. Phys Rev B 2006:73.
[55] Moser B, Kuebler J, Meinhard H, Muster W, Michler J. Observation of instabilities during plastic deformation by in-situ SEM indentation experiments. Adv Eng Mater 2005;7:388.
[56] Schuh CA, Nieh TG. A nanoindentation study of serrated flow in bulk metallic glasses. Acta Mater 2003;51:87.
[57] Schuh CA, Nieh TG. A survey of instrumented indentation studies on metallic glasses. J Mater Res 2004;19:46.
[58] Bahr DF, Wilson DE, Crowson DA. Energy considerations regarding yield points during indentation. J Mater Res 1999;14:2269.
[59] Bei H, Lu ZP, George EP. Theoretical strength and the onset of plasticity in bulk metallic glasses investigated by nanoindentation with a spherical indenter. Phys Rev Lett 2004:93.
[60] Lund AC, Hodge AM, Schuh CA. Incipient plasticity during nanoindentation at elevated temperatures. Appl Phys Lett 2004;85:1362.
[61] Moser B, Loffler JF, Michler J. Discrete deformation in amorphous metals: an in situ SEM indentation study. Philos Mag 2006;86:5715.
[62] Fischer-Cripps AC. Introduction to contact mechanics. New York: Springer; 2000.
[63] Johnson KL. Contact mechanics. Cambridge [Cambridgeshire]; New York: Cambridge University Press; 1985.
[64] Bhushan B. Handbook of micro/nano tribology. Boca Raton: CRC Press; 1999.
[65] Chen QJ, Shen J, Zhang DL, Fan HB, Sun JF. Mechanical performance and fracture behavior of $Fe_{41}Co_7Cr_{15}Mo_{14}Y_2C_{15}B_6$ bulk metallic glass. J Mater Res 2007;22:358.
[66] Fu XL, Li Y, Schuh CA. Mechanical properties of metallic glass matrix composites: effects of reinforcement character and connectivity. Scripta Mater 2007;56:617.
[67] Desai CS, Siriwardane HJ. Constitutive laws for engineering materials, with emphasis on geologic materials. Englewood Cliffs, N.J: Prentice-Hall; 1984.
[68] Ramamurty U, Jana S, Kawamura Y, Chattopadhyay K. Hardness and plastic deformation in a bulk metallic glass. Acta Mater 2005;53:705.
[69] Antoniou A, Bastawros A, Biner B. Experimental observations of deformation behavior of bulk metallic glasses during wedge-like cylindrical indentation. J Mater Res 2007;22:514.
[70] Antoniou A, Bastawros AF, Lo CCH, Biner SB. Deformation behavior of a zirconium based metallic glass during cylindrical indentation: in situ observations. Mater Sci Eng A 2005;394:96.
[71] Su C, Anand L. Plane strain indentation of a Zr-based metallic glass: experiments and numerical simulation. Acta Mater 2006;54:179.
[72] Zhang HW, Jing XN, Subhash G, Kecskes LJ, Dowding RJ. Investigation of shear band evolution in amorphous alloys beneath a Vickers indentation. Acta Mater 2005;53:3849.
[73] Bahr DF, Vasquez G. Effect of solid solution impurities on dislocation nucleation during nanoindentation. J Mater Res 2005;20:1947.
[74] Michalske TA, Houston JE. Dislocation nucleation at nano-scale mechanical contacts. Acta Mater 1998;46:391.
[75] Schuh CA, Lund AC. Application of nucleation theory to the rate dependence of incipient plasticity during nanoindentation. J Mater Res 2004;19:2152.
[76] Suresh S, Nieh TG, Choi BW. Nano-indentation of copper thin films on silicon substrates. Scripta Mater 1999;41:951.
[77] Wang W, Jiang CB, Lu K. Deformation behavior of Ni_3Al single crystals during nanoindentation. Acta Mater 2003;51:6169.
[78] Hertz H. Miscellaneous papers. London: Macmillan; 1896.
[79] Lund AC, Schuh CA. Yield surface of a simulated metallic glass. Acta Mater 2003;51:5399.
[80] Zhang ZF, He G, Eckert J, Schultz L. Fracture mechanisms in bulk metallic glassy materials. Phys Rev Lett 2003;91:045505.
[81] Patnaik MNM, Narasimhan R, Ramamurty U. Spherical indentation response of metallic glasses. Acta Mater 2004;52:3335.
[82] Wright WJ, Saha R, Nix WD. Deformation mechanisms of the $Zr_{40}Ti_{14}Ni_{10}Cu_{12}Be_{24}$ bulk metallic glass, vol. 42. Singapore: Japan Inst. Metals; 2001. p. 642.
[83] Anand L, Su C. A theory for amorphous viscoplastic materials undergoing finite deformations, with application to metallic glasses. J Mech Phys Solids 2005;53:1362.
[84] Jana S, Bhowmick R, Kawamura Y, Chattopadhyay K, Ramamurty U. Deformation morphology underneath the Vickers indent in a Zr-based bulk metallic glass. Intermetallics 2004;12:1097.
[85] Keryvin V. Indentation of bulk metallic glasses: relationships between shear bands observed around the prints and hardness. Acta Mater 2007;55:2565.
[86] Zhang H, Jing X, Subhash G, Kecskes LJ, Dowding RJ. Investigation of shear band evolution in amorphous alloys beneath a Vickers indentation. Acta Mater 2005;53:3849.
[87] Alpas AT, Edwards L, Reid CN. Fracture and fatigue crack-propagation in a nickel-base metallic-glass. Metall Trans A 1989;20:1395.
[88] Jeong HY, Li XW, Yee AF, Pan J. Slip lines in front of a round notch tip in a pressure-sensitive material. Mech Mater 1994;19:29.
[89] Al-Abduljabbar A, Pan J. Effects of pressure sensitivity and notch geometry on notch-tip fields. Polym Eng Sci 1998;38:1031.
[90] Lambson EF, Lambson WA, Macdonald JE, Gibbs MRJ, Saunders GA, Turnbull D. Elastic behavior and vibrational anharmonicity of a bulk $Pd_{40}Ni_{40}P_{20}$ metallic glass. Phys Rev B 1986;33:2380.
[91] Wang WH. Correlations between elastic moduli and properties in bulk metallic glasses. J Appl Phys 2006;99:093506.